Compact Object Mergers Driven by Gas Fallback

Hiromichi Tagawa,[1,*] Takayuki R. Saitoh,[2] and Bence Kocsis[1]
[1]*Institute of Physics, Eötvös University, Pázmány P.s., Budapest 1117, Hungary*
[2]*Earth-Life Science Institute, Tokyo Institute of Technology, 2-12-1, Ookayama, Meguro, Tokyo 152-8551, Japan*

(Received 2 February 2018; revised manuscript received 10 April 2018; published 25 June 2018)

Recently, several gravitational wave detections have shown evidence for compact object mergers. However, the astrophysical origin of merging binaries is not well understood. Stellar binaries are typically at much larger separations than what is needed for the binaries to merge due to gravitational wave emission, which leads to the so-called final AU problem. In this Letter we propose a new channel for mergers of compact object binaries which solves the final AU problem. We examine the binary evolution following gas expansion due to a weak failed supernova explosion, neutrino mass loss, core disturbance, or envelope instability. In such situations the binary is possibly hardened by ambient gas. We investigate the evolution of the binary system after a shock has propagated by performing smoothed particle hydrodynamics simulations. We find that significant binary hardening occurs when the gas mass bound to the binary exceeds that of the compact objects. This mechanism represents a new possibility for the pathway to mergers for gravitational wave events.

DOI: 10.1103/PhysRevLett.120.261101

Introduction.—Recent gravitational wave (GW) detections show evidence for a high rate of black hole (BH)-BH and neutron star (NS)-NS mergers in the Universe [1–5]. However, the proposed astrophysical pathways to mergers remain highly debated. Although several channels for the formation of close binaries have been proposed [6], it is not obvious how separations are reduced for various types of binaries until merging due to gravitational wave emission, which leads to the so-called final AU problem [7]. The major pathways to solve this problem are the common envelope (CE) evolution which operates for 0.01-several AU separations. Although the binary separation can be largely reduced by the CE evolution, the final separations of the post CE binaries are not well understood [8,9]. To reproduce the compact object mergers or x-ray binaries, the CE phase needs to end at some appropriate separation. However, many of the observed x-ray binaries are difficult to reproduce with the CE model; see Ref. [10] and references therein.

Here we propose a new hardening channel for mergers of compact object binaries which solves the final AU problem. We focus on the environments after the stellar envelope expands. Such a situation is expected in a weak supernova followed by fallback accretion, which is thought to occur for zero-age main sequence progenitors of masses above $\sim$10–15 $M_\odot$ [11–14]. Further, when the explosion fails, mass loss due to a neutrino emission during a protoneutron star phase [15–17] causes an outgoing sound pulse which grows into a shock and ejects some outer material [18]. Also, prior to core collapse, the hydrogen envelope may expand due to core disturbance [19] or envelope instability [20]. Such precollapse expansion is observed as the luminous blue variables [21] or type IIn supernovae, which are accompanied by an expanded envelope within $\lesssim$100 AU and are $\sim$10% of all core-collapse events [22]. In all these cases, as the gas expands and falls back, gas may exist abundantly at a large distance from the forming compact object.

If a significant amount of gas settles around a binary, gas driven binary hardening occurs, either by dynamical friction (DF) [23–26], similar to that in the CE evolution, or via resonant disk migration [27–29]. The remarkable differences of the gas expansion and fallback scenario from the CE model are that binaries with separations of larger than several AU can merge due to the extended gas distribution and the merger may take place soon after this gas-driven evolutionary phase. In this Letter, we investigate how the binary evolves after gas expands and identify the range of astrophysically important parameters required for a merger.

Method.—To simulate the binary evolution interacting with ambient gas, we use an N-body or smoothed particle hydrodynamics (SPH) code, ASURA [30,31]. Gas dynamics is solved using the density-independent SPH (DISPH) method [32] with an ideal gas equation of state. We adopt a shared time step as the minimum of a hydrodynamical and a gravitational time step for gaseous particles [33] and a gravitational time step for the binary [34].

We refer to both the explosion remnant (primary) and the companion (secondary) as compact objects (COs), which may be BHs, NSs, white dwarfs, or steller cores. Gravitational interaction among gas-gas particles is solved by a parallel tree with gravity pipe method [35], while that between CO-gas and CO-CO is solved by a direct summation. The CO is

modeled as a point mass which interacts only gravitationally with other particles. We set gravitational softening lengths to prevent numerical divergences during close approaches to $\sqrt{2}\epsilon$, ϵ, and 0 for gas-gas particles, gas-CO, and CO-CO interactions, respectively [36].

Setup of simulations.—Just after neutrino mass loss [16,17] or precollapse expansion [19,20], or before fallback accretion [14,37], a shock propagates to the stellar envelope and the envelope expands homologously. We start the simulation after a shock has propagated, referring to the study about fallback accretion by Zampieri *et al.* [38]. Initially we set the separation between the two COs to $a_{\rm ini}$. At the beginning of the evolution, the gas cloud has homogeneous density within a minimum $r_{\rm min} = 0.1$ AU and maximum radius $r_{\rm max} = 0.2$ AU from the primary. The gas has an outgoing radial velocity profile of $v(r) = f_{\rm v} v_{\rm max} r/r_{\rm max}$ from the primary with $v_{\rm max} = |2\Phi_{\rm pri}(r_{\rm max})|$ $0.5 \sim 220$ km/s$(M_{\rm CO,ini}/5\ M_\odot)(r_{\rm max}/0.2\ {\rm AU})^{-1}$, where $\Phi_{\rm pri}(r)$ is the gravitational potential of the primary, r is the radial distance from the primary, and $M_{\rm CO,ini}$ is the initial CO mass.

For simplicity, we initially rotate the binary COs and gas particles around the center of mass of the bound system after an initial expansion.

In our simulations, gas accretes onto a CO when the gas has inward motion toward the CO, the gas is within ϵ from the CO, and the specific angular momentum of the gas relative to the CO is lower than the specific Keplerian angular momentum at the last stable circular orbit of a Schwarzschild BH as in studies of disk formation after fallback accretion [39,40]. We run additional simulations without accretion onto the COs for comparison, which may resemble the case of strong radiation feedback, the rotation of progenitors, or precollapse expansion. After precollapse expansion, the stellar core plays the role of the primary so the nearby gas is stabilized by gas pressure as in the standard CE evolution. In the case without accretion, the gas within ϵ of the CO is not removed, although its gravitational effects are reduced by the softening. The simulation is stopped if the binary separation becomes smaller than ϵ.

For the fiducial model, we set the initial CO mass $M_{\rm CO,ini} = 5\ M_\odot$, the initial binary semimajor axis $a_{\rm ini} = 3$ AU, the initial gas temperature $T_{\rm ini} = 2 \times 10^6$ K, the initial gas mass $M_{\rm gas,ini} = 10\ M_\odot$, the gravitational softening length $\epsilon = 0.1$ AU, the artificial viscous strength $\alpha_{\rm sph} = 0.4$, see Eq. (46) in Ref. [32], the specific heat ratio [32] of $\gamma = 5/3$, the SPH particle number $N = 3 \times 10^4$, and the neighbor number setting the kernel size of each SPH particle to be 32 ± 2. Both the primary and secondary CO masses $M_{\rm CO1}$ and $M_{\rm CO2}$ are initially set to $M_{\rm CO,ini}$. The assumed CO and gas masses correspond to zero age main sequence progenitors with mass of 15–30 $M_\odot$, whose final helium core mass is $\sim 5\ M_\odot$ and final hydrogen mass is $\gtrsim 10\ M_\odot$ [11]. We set $T_{\rm ini}$ using the initial sonic velocity $c_{\rm s}$ ($\sim$140 km/s) at $r_{\rm max} = 3 \times 10^{12}$ cm, consistent with a recent study of gas dynamics following neutrino mass loss ($\sim$100–500 km/s [16]). Furthermore, $\alpha_{\rm sph} = 0.4$ corresponds to the viscous parameter in the α prescription [41] of $\alpha_{\rm ss} \sim 0.005$ [42] at $r \sim a_{\rm ini}$. We verify that the number of particles is sufficient to resolve $\epsilon = 0.1$ AU around the primary since the kernel size of SPH particles at $r \sim 0.1$ AU is $\sim$0.02 AU.

Dynamics of binary evolution.—We first present the binary evolution in the fiducial model without gas accretion onto COs. Figure 1 shows the snapshots of the gas density distribution, and Fig. 2 shows the time evolution of the various physical quantities for the fiducial models. At $t =$ 0.1 yr of Fig. 1 gas just around the primary ($\lesssim$1) falls back and is stabilized by gas pressure but the gas around the secondary is still expanding. Then, a gas envelope forms around the secondary as seen in $t = 1$ yr of Fig. 1. At this time, the Bondi-Hoyle-Lyttleton radius of the secondary is $\sim$2 AU and the masses of envelopes mainly bound to the primary and secondary are $\sim 5.1\ M_\odot$ and $0.3\ M_\odot$, respectively. Zampieri *et al.* [38] indicated that there is little difference in the gas dynamics during fallback accretion between radiation-dominated completely ionized hydrogen gas and a polytropic gas with no radiation. We verify that the gas dynamics at $\sim$1 yr in our simulation is consistent with minor differences in the density profile with respect to

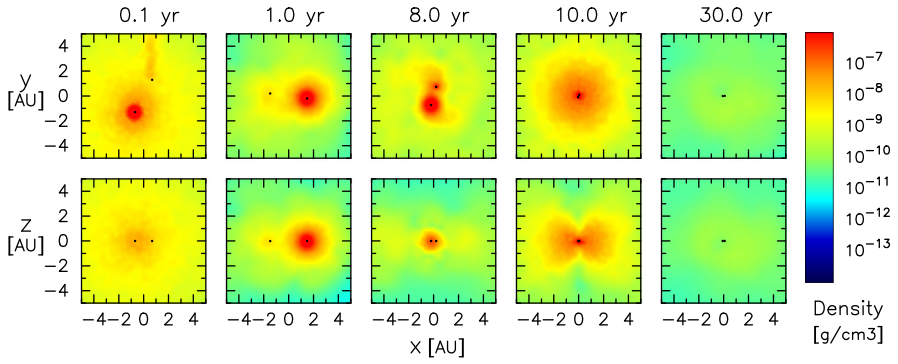

FIG. 1. The gas density maps for the fiducial model without accretion at $t = 0.1$, 1, 8, 10, and 30 yr. Upper and lower panels are in the x-y (orbital) and x-z planes, respectively. Black points represent the position of compact objects.

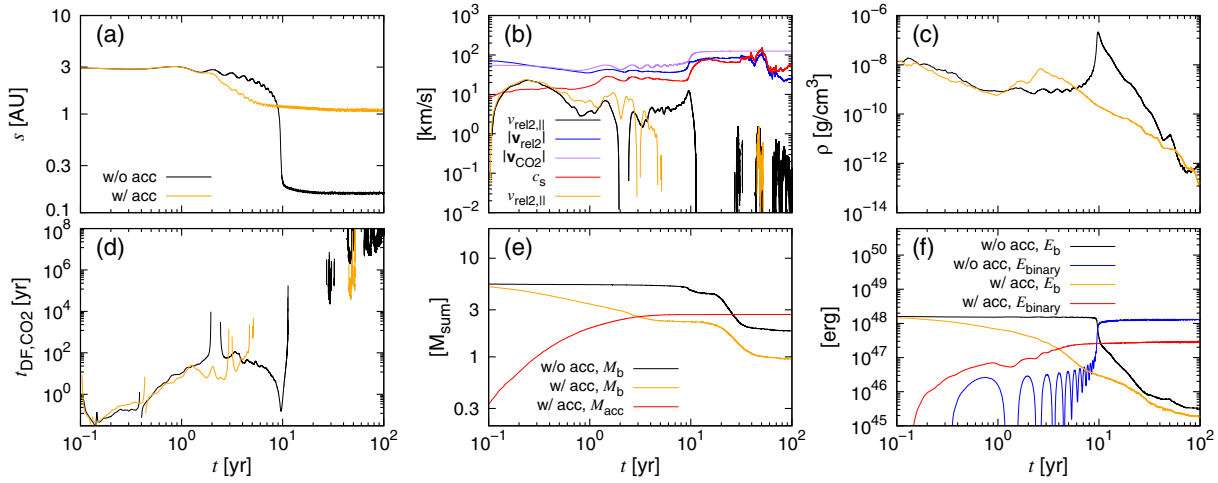

FIG. 2. Panels (a),(c),(d), and (e) show the evolution of the binary separation, the gas density, the dynamical friction timescale, and the bound gas mass, respectively, for the models without (black) and with (orange) accretion. Gas properties are averaged within 1–5 BHL radii of the secondary (see text). Blue, black, purple, and red lines in panel (b) are the relative gas velocity with respect to the secondary, its component along the secondary velocity $v_{\mathrm{rel2},\parallel}$, the secondary velocity, and the sonic velocity for the model without accretion; the orange line shows $v_{\mathrm{rel2},\parallel}$ for the model with accretion. Red line in panel (e) represents the accreted mass for the model with accretion. Panel (f) shows the binding energy for the bound gas without (black) and with (orange) accretion. and the binary orbital energy without (blue) and with (red) accretion.

Ref. [38]. After the gas settles, the binary is hardened by DF, i.e., the gravitational force of the density wake seen as tidal streamlike structures at $t = 8$ yr of Fig. 1. This causes the binary separation [black line in panel (a) of Fig. 2] to rapidly decrease as seen in $t \sim 10$ yr. During binary hardening, the gas binding energy is transferred to the binary orbital energy [black and blue lines in panels (f) of Fig. 2, respectively]. Finally, the gas expands (10 and 30 yr of Fig. 1) and the binary hardening almost stops [black line in panel (a) of Fig. 2].

To verify whether the main hardening mechanism is DF, we compare $t_{\mathrm{hard}} \sim 10$ yr to the DF timescale, where we define t_{hard} is the time for the binary separation to shrink to the geometric mean of a_{ini} and a_{fin}. Here we derive the DF timescale for the secondary, which has the larger velocity and angular momentum among the COs, which must be transferred to the gas for the binary to harden. Since DF is the gravitational force mostly from outside of the Bondi-Hoyle-Lyttleton (BHL) radius, the physical quantities, $v_{\mathrm{rel2},\parallel}$, $|\mathbf{v}_{\mathrm{rel2}}|$, c_s, and ρ, (see Fig. 2 for definition) are *ad hoc* averaged for the gas between 1 and 5 BHL radii of the secondary and outside of the BHL radius of the primary. The DF timescale for the secondary $t_{\mathrm{DF,CO2}} \equiv |\mathbf{v}_{\mathrm{CO2}}|/a_{\mathrm{DF,CO2}}$ [black line in panel (d) of Fig. 2] is calculated using the analytic formulas of the DF acceleration derived by Ostriker [43], where $a_{\mathrm{DF,CO2}}$ is the DF acceleration for the secondary. We use $v_{\mathrm{rel2},\parallel}$ instead of $|\mathbf{v}_{\mathrm{rel2}}|$ in $a_{\mathrm{DF,CO2}}$ since the binary orbital decay due to DF is mostly caused by the force from the parallel direction to the CO motion [44]. As seen in panel (d) of Fig. 2, $t_{\mathrm{hard}} \sim 10$ yr is well matched to $t_{\mathrm{DF,CO2}}$ although $t_{\mathrm{DF,CO2}}$ exhibits large fluctuations due to the binary's orbital motion.

On the other hand, in the models with accretion, t_{hard} is smaller than that without accretion [panel (a) of Fig. 2]. This is because t_{hard} is shortened by the increase of $v_{\mathrm{rel2},\parallel}$ due to gas accretion. Although $v_{\mathrm{rel2},\parallel}$ is reduced compared to $|\mathbf{v}_{\mathrm{rel2}}|$ by the angular momentum transfer due to the DF at ~0.1–2 yr, this reduction is small in the model with accretion [black and orange lines in panel (b) of Fig. 2]. This comes from the inward motion of accreting gas in the cases with accretion. Since $v_{\mathrm{rel2},\parallel}$ is subsonic, the increase in $v_{\mathrm{rel2},\parallel}$ enhances the drag force [43]. Thus since accretion makes DF more efficient, the binary hardening starts earlier during the accretion period of $\lesssim 5$ yr [panels (a), (d), and (e) of Fig. 2] in the cases with accretion.

Energy formalism.—The final fate of the binary evolution may be determined as a function of physical parameters following the energy formalism commonly used for CE. In particular, a_{fin} is predicted as

$$\begin{aligned}&\alpha[G(M_{\mathrm{CO1,fin}} + M_{\mathrm{b,fin}})M_{\mathrm{CO2,fin}}/(2a_{\mathrm{fin}}) \\ &\quad - G(M_{\mathrm{CO1,fin}} + M_{\mathrm{b,ini}})M_{\mathrm{CO2,fin}}/(2a_{\mathrm{ini}})] \\ &\quad = G(M_{\mathrm{CO1,fin}} + M_{\mathrm{b,ini}})(M_{\mathrm{b,ini}})/(\lambda R_{\mathrm{rlof1}}) \qquad (1)\end{aligned}$$

[8,45,46], where α is the parameter that describes the efficiency of transferring the energy of the bound gas, λ represents the typical size of the gas bound to the primary compared to R_{rlof1}, the radius of Roche lobe around the primary [47], G is the gravitational constant, $M_{\mathrm{CO1,fin}}$ and $M_{\mathrm{CO2,fin}}$ are the final primary and secondary mass, $M_{\mathrm{b,fin}}$ is

the final bound gas mass, $M_{\rm b,ini} = M_{\rm b,fin} + M_{\rm ej}$ is the initial bound gas mass, and $M_{\rm ej}$ is the ejected gas mass. We use $M_{\rm ej}$ after the potential energy of bound gas reaches its maximum at $\sim$1 yr to reduce the contribution to Eq. (1) by an initial expansion. To investigate the dependence on $\alpha\lambda R_{\rm rlof1}$, we perform additional simulations for 4 models whose different parameters to the fiducial models with and without accretion are $a_{\rm ini} = 2$ and 5 AU, respectively. We derive fitting models, $\alpha\lambda R_{\rm rlof1} \propto a_{\rm ini}^{0}$ and $\alpha\lambda R_{\rm rlof1} \propto a_{\rm ini}^{1.2}$ for the models without and with accretion, respectively. In the cases with accretion, large $a_{\rm ini}$ increases α due to the reduction of the contribution of DF to the energy loss of gas. This reduction may be caused by the increase in accreted mass due to the decrease of the gravitational torque from the secondary, and the reduced DF acceleration due to the low gas density around the binary. Both effects make the ratio of the energy loss by DF to that by accretion smaller. Using this result, we derive Fig. 3, which shows the merger criterion as a function of initial parameters, Eq. (1) for different $M_{\rm CO,ini}$ and accretion models. According to Fig. 3, gas accretion has a large impact on hardening especially for large $a_{\rm ini}$. The final fate of the binary is determined by the bound gas mass, which is well predicted by the ratio of the gravitational energy over the kinetic plus thermal energy. Here, in the fiducial model with and without accretion, $M_{\rm b,ini} = 5.4$ and 2.7 $M_\odot$, respectively, $M_{\rm ej} = 3.7$ and 1.8 $M_\odot$, and $M_{\rm b,fin} = 1.7$ and 0.9 $M_\odot$. When the initial expansion velocity is uniformly increased by 50% and 100%, $M_{\rm b,ini}$ is, respectively, decreased by $\sim$30% and $\sim$60% in both cases with and without accretion. Also, when setting the initial gas density profile to be $\rho_{\rm ini}(r) \propto r^{-3}$, $M_{\rm b,ini}$ is decreased by $\sim$20% and increased by $\sim$10% in the cases with and without accretion, respectively, relative to that for $\rho_{\rm ini}(r) \propto$ const. In all of these cases, since the changes in $\alpha\lambda R_{\rm rlof1}$ are modest, the degree of migration is predicted via Eq. (1) and Fig. 3 applies to show the condition for merger.

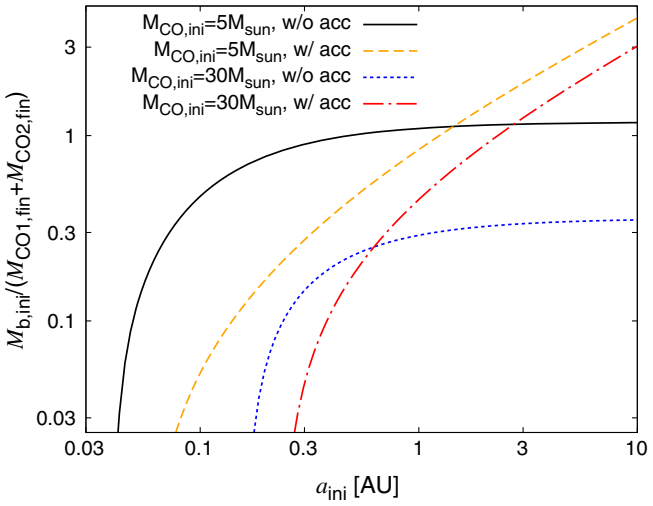

FIG. 3. The criterion for the ratio of the initial bound gas mass to the initial binary mass above which the merger occurs within the Hubble time: $a_{\rm fin} \lesssim 0.05$ AU$(M_{\rm CO1}/5\ M_\odot)^{1/4}$ $(M_{\rm CO2}/5\ M_\odot)^{1/4}[(M_{\rm CO1}+M_{\rm CO2})/10\ M_\odot]^{1/4}$, assuming zero binary eccentricity for a final GW-driven merger [48]. Lines are calculated using Eq. (1), where $\alpha\lambda R_{\rm rlof1}$ is obtained from the simulation results, extrapolated by the derived relation between $\alpha\lambda R_{\rm rlof1}$ and $a_{\rm ini}$. Black and blue dashed lines show results for the fiducial models without and with accretion, respectively. Orange dotted and red dash-dotted lines show results for $M_{\rm CO1,ini} = M_{\rm CO2,ini} = 30\ M_\odot$ without and with accretion, respectively.

In the cases with gas accretion, the hardening rate has an upper bound since the ratio of the bound gas mass to the accreted mass approaches a constant as the initial gas mass increases in our settings. As a result, the reduction of the semi-major axis is found to be less than $\sim$5 when $M_{\rm CO,ini} = 5\ M_\odot$. On the other hand, in cases with negligible accretion such as for precollapse expansion, the hardening can be significant. Here the time lag between precollapse expansion and the type IIn supernova is predicted to be $\sim$1000 yr at most [20]. By performing some additional simulations, in which the values of $a_{\rm ini}$ and $M_{\rm gas}$ are different from the fiducial model, we derive the fitting relation $t_{\rm DF,CO2} \propto \sim a_{\rm ini}^{3.0} M_{\rm b,ini}^{0.3}$ for $M_{\rm b,ini} \gtrsim M_{\rm b,cri}$ where $M_{\rm b,cri} \sim 7\ M_\odot (a_{\rm ini}/{\rm AU})^{0.6}$. Using this relation, the mergers within 1000 yr without accretion for $M_{\rm CO,ini} = 5\ M_\odot$ require $a_{\rm ini} \lesssim 15$ AU$(t_{\rm hard}/1000\ {\rm yr})^{0.33}$ $(M_{\rm b,ini}/M_{\rm b,cri})^{-0.1}$. Thus, there is a possibility that binaries with large separations within $\sim$15 AU can merge after precollapse expansion.

The NS-NS merger rate inferred from the GW170817 event ($\gtrsim 1\ {\rm yr}^{-1}$ within 100 Mpc) is much larger than those estimated for the major merger channels such as isolated binary ($\sim 6 \times 10^{-2}\ {\rm yr}^{-1}$) and dynamical evolution ($\sim 2 \times 10^{-4}\ {\rm yr}^{-1}$) models [49]. Thus, an additional merger channel may need to be proposed to explain the observed rate [50]. Gas fallback driven mergers allow wider ranges of the initial separations for mergers. Natal kicks, which reduce the merger rate by about 1 order of magnitude [53] for isolated binaries, are small in cases of neutrino mass loss which may lead to gas fallback driven mergers. Thus, this channel has a potential to be highly relevant for NS-NS mergers. In particular, significant hardening should be caused by precollapse expansion for the remnants to remain NSs until the merger.

Conclusions.—We conclude that compact object mergers may be common in cases where a significant amount of gas is released by the progenitor in the region surrounding the binary. The required gas mass bound to the binary must typically exceed the mass of the compact objects. For a 10 $M_\odot$ binary, a gas-assisted merger can occur if the initial separation is $\lesssim$15 AU, and in cases where the COs accrete, the gas-driven reduction in the semimajor axis is $\lesssim$5. We highlighted some processes that can possibly lead to these

conditions, but further investigations are needed to understand the most common circumstances of this merger channel. Mergers facilitated by the progenitors' envelope expansion may leave an imprint on the mass and mass-ratio distribution of merger rates, which will be obtained using GW detections.

We thank Scott Tremaine and Enrico Ramirez-Ruiz for useful comments. We are also grateful to the anonymous referees for important remarks. This work received funding from the European Research Council under the EU's Horizon 2020 research and innovation programme, Grant Agreement No. 638435 and by NKFIH KH-125675. Simulations and analyses were carried out on Cray XC30 and computers at the Center for Computational Astrophysics, National Astronomical Observatory of Japan.

*htagawa@caesar.elte.hu

[1] B. P. Abbott *et al.*, Phys. Rev. Lett. **116**, 061102 (2016).
[2] B. P. Abbott *et al.*, Phys. Rev. Lett. **116**, 241103 (2016).
[3] B. P. Abbott *et al.*, Phys. Rev. Lett. **118**, 221101 (2017).
[4] LIGO Scientific Collaboration *et al.*, Phys. Rev. Lett. **119**, 141101 (2017).
[5] LIGO Scientific Collaboration *et al.*, Astrophys. J. **848**, L13 (2017).
[6] K. M. Kratter, *Evolution of compact binaries. Proceedings of a workshop held at Hotel San Martín, Viña del Mar, Chile, 2011* (Astronomical Society of the Pacific, San Francisco, 2011), p. 47.
[7] N. C. Stone, B. D. Metzger, and Z. Haiman, Mon. Not. R. Astron. Soc. **464**, 946 (2017).
[8] N. Ivanova *et al.*, Astron. Astrophys. Rev. **21**, 59 (2013).
[9] E. Sabach, S. Hillel, R. Schreier, and N. Soker, Mon. Not. R. Astron. Soc. **472**, 4361 (2017).
[10] P. Podsiadlowski, S. Rappaport, and Z. Han, Mon. Not. R. Astron. Soc. **341**, 385 (2003).
[11] T. Sukhbold, T. Ertl, S. E. Woosley, J. M. Brown, and H.-T. Janka, Astrophys. J. **821**, 38 (2016).
[12] C. A. Raithel, T. Sukhbold, and F. Ozel, Astrophys. J. **856**, 35 (2018).
[13] C. L. Fryer, K. Belcynski, G. Wiktorowicz, M. Dominik, V. Kalogera, and D. E. Holz, Astrophys. J. **749**, 91 (2012).
[14] S. E. Woosley and T. A. Weaver, Astrophys. J. Suppl. Ser. **101**, 181 (1995).
[15] E. O'Connor and C. D. Ott, Astrophys. J. **762**, 126 (2013).
[16] R. Fernandez, E. Quataert, K. Kashiyama, and E. R. Coughlin, Mon. Not. R. Astron. Soc. **476**, 2366 (2018).
[17] E. R. Coughlin, E. Quataert, R. Fernandez, and D. Kasen, Mon. Not. R. Astron. Soc. **477**, 1225 (2018).
[18] E. Lovegrove and S. E. Woosley, Astrophys. J. **769**, 109 (2013).
[19] J. H. Shiode and E. Quataert, Astrophys. J. **780**, 96 (2014).
[20] N. Smith and W. D. Arnett, Astrophys. J. **785**, 82 (2014).
[21] N. Smith, W. Li, J. M. Silverman, M. Ganeshalingam, and A. V. Filippenko, Mon. Not. R. Astron. Soc. **415**, 773 (2011).
[22] N. Smith, W. Li, A. V. Filippenko, and R. Chornock, Mon. Not. R. Astron. Soc. **412**, 1522 (2011).
[23] A. Escala, R. B. Larson, P. S. Coppi, and D. Mardones, Astrophys. J. **607**, 765 (2004).
[24] D. Chapon, L. Mayer, and R. Teyssier, Mon. Not. R. Astron. Soc. **429**, 3114 (2013).
[25] H. Tagawa, M. Umemura, N. Gouda, T. Yano, and Y. Yamai, Mon. Not. R. Astron. Soc. **451**, 2174 (2015).
[26] H. Tagawa and M. Umemura, Astrophys. J. **856**, 47 (2018).
[27] P. Goldreich and S. Tremaine, Astrophys. J. **241**, 425 (1980).
[28] B. Kocsis, N. Yunes, and A. Loeb, Phys. Rev. D **84**, 024032 (2011).
[29] Y. Tang, A. MacFadyen, and Z. Haiman, Mon. Not. R. Astron. Soc. **469**, 4258 (2017).
[30] T. R. Saitoh, H. Daisaka, E. Kokubo, J. Makino, T. Okamoto, K. Tomisaka, K. Wada, and N. Yoshida, Publ. Astron. Soc. Jpn. **60**, 667 (2008).
[31] T. R. Saitoh, H. Daisaka, E. Kokubo, J. Makino, T. Okamoto, K. Tomisaka, K. Wada, and N. Yoshida, Publ. Astron. Soc. Jpn. **61**, 481 (2009).
[32] T. R. Saitoh and J. Makino, Astrophys. J. **768**, 44 (2013).
[33] T. R. Saitoh and J. Makino, Publ. Astron. Soc. Jpn. **62**, 301 (2010).
[34] C. Baruteau, J. Cuadra, and D. N. C. Lin, Astrophys. J. **726**, 28 (2011).
[35] J. Makino, Publ. Astron. Soc. Jpn. **56**, 521 (2004).
[36] T. R. Saitoh and J. Makino, New Astron., **17**, 76 (2012).
[37] A. Batta, E. Ramirez-Ruiz, and C. Fryer, Astrophys. J. Lett. **846**, L15 (2017).
[38] L. Zampieri, M. Colpi, S. L. Shapiro, and I. Wasserman, Astrophys. J. **505**, 876 (1998).
[39] R. Perna, P. Duffell, M. Cantiello, and A. I. MacFadyen, Astrophys. J. **781**, 119 (2014).
[40] S. E. Woosley and A. Heger, Astrophys. J. **752**, 32 (2012).
[41] N. I. Shakura and R. A. Sunyaev, Astron. Astrophys. **24**, 337 (1973).
[42] Z. Meglicki, D. Wickramasinghe, and G. V. Bicknell, Mon. Not. R. Astron. Soc. **264**, 691 (1993).
[43] E. C. Ostriker, Astrophys. J. **513**, 252 (1999).
[44] H. Kim and W.-T. Kim, Astrophys. J. **665**, 432 (2007).
[45] M. de Kool, Astrophys. J. **358**, 189 (1990).
[46] R. F. Webbink, Astrophys. J. **277**, 355 (1984).
[47] P. P. Eggleton, Astrophys. J. **268**, 368 (1983).
[48] P. C. Peters, Phys. Rev. **136**, B1224 (1964).
[49] K. Belczynski, A. Askar, M. Arca-Sedda, M. Chruslinska, M. Donnari, M. Giersz, M. Benacquista, R. Spurzem, D. Jin, G. Wiktorowicz, and D. Belloni, arXiv:1712.00632 [Astron. Astrophys. (to be published)].
[50] Some estimates claim to explain the merger rate [51,52].
[51] K. Hotokezaka and T. Piran, Astrophys. J. **842**, 111 (2017).
[52] K. Hotokezaka, P. Beniamini, and T. Piran, arXiv: 180101141.
[53] K. Belczynski, V. Kalogera, and T. Bulik, Astrophys. J. **572**, 407 (2002).